Processing and Fabrication of Advanced Materials - XIX

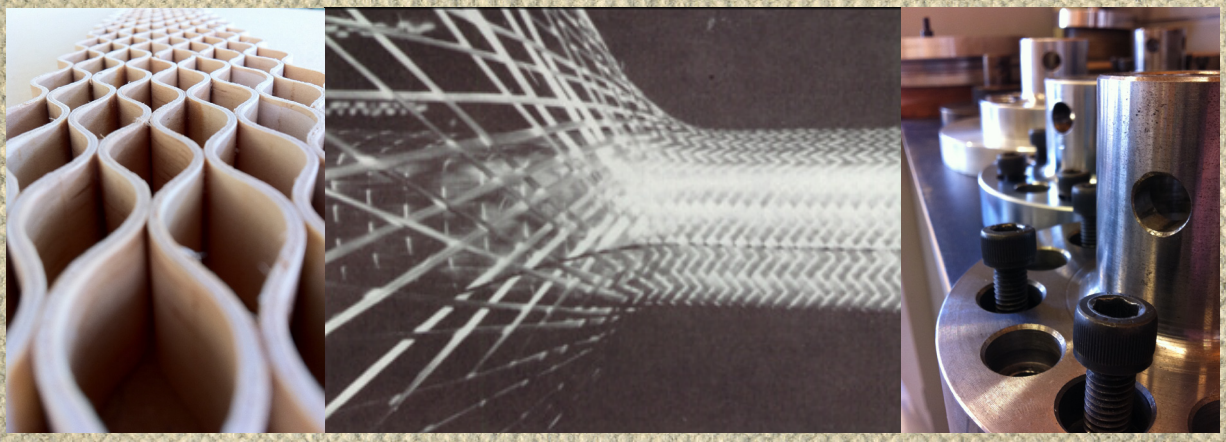

Auckland, New Zealand, January 2011

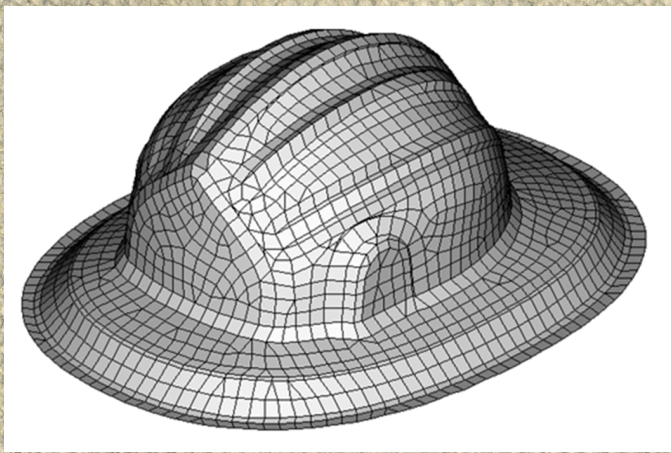

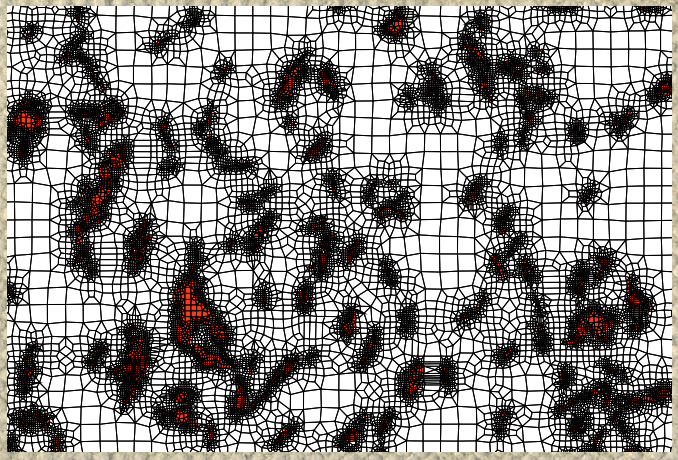

Editors:
D. Bhattacharyya
R.J.T. Lin
T.S. Srivatsan

Processing and Fabrication of Advanced Materials XIX

Editors:
D. Bhattacharyya
R.J.T. Lin
T.S. Srivatsan

Processing and Fabrication of Advanced Materials XIX

Proceedings of an International Conference organized by:

The Centre for Advanced Composite Materials
The University of Auckland
New Zealand

January 14-17, 2011

The University of Auckland
Auckland, New Zealand

Hard copy: ISBN 978-0-473-18178-9 (set)
Electronic copy: ISBN 978-0-473-18189-5

Preface

These volumes contain the papers presented at the ***Nineteenth International Conference on Processing and Fabrication of Advanced Materials (PFAM XIX)*** held in Auckland, New Zealand, during **January 14-17, 2011**. The ***Centre for Advanced Composite Materials housed within the Faculty of Engineering***, at **the University of Auckland** (Auckland, New Zealand), was the principal organiser that put together this international conference spread over four days. It is the NINETEENTH in a series of conferences bringing together engineers, technologists, and researchers from industry, universities and research laboratories, working on various aspects related to the processing, fabrication, characterisation and evaluation of both advanced and emerging materials. The idea is to share and discuss their research findings, observations and inferences. The earlier conferences were held as follows:

(1) The ***first*** was held in Cincinnati (USA) in **1991**
(2) The ***second*** was held in Chicago (USA) in **1992**
(3) The ***third*** was held in Pittsburgh (USA) in **1993**
(4) The ***fourth*** in Cleveland (USA) in **1995**
(5) The ***fifth*** in Cincinnati (USA) in **1996**
(6) The ***sixth*** in Singapore (Singapore) in **1997**
(7) The ***seventh*** was held in Rosemont, Illinois (USA) in **1998**
(8) The ***eighth*** was held in Singapore (Singapore) in **1999**
(9) The ***ninth*** was held in St. Louis, Missouri (USA) in **2000**
(10) The ***tenth*** was held in Indianapolis, Indiana (USA) in **2001**
(11) The ***eleventh*** was held in Columbus, Ohio (USA) in **2002**
(12) The ***twelfth*** was held at Pittsburgh, PA (USA) in **2003**
(13) The ***thirteenth*** was held in Singapore (Singapore) in **2004**
(14) The ***fourteenth*** was held in Pittsburgh, PA (USA) in **2005**
(15) The ***fifteenth*** was held in Cincinnati, OH (USA) in **2006**
(16) The ***sixteenth*** was held in Singapore (Singapore) in **2007**
(17) The ***seventeenth*** was held in New Delhi (India) in **2008.**
(18) The ***eighteenth*** was held in Sendai (Japan) in **2009.**

This conference is a collection of papers from over 30 countries. Over 200 abstracts that include both invited and contributed papers, were received and reviewed for oral/poster presentations. More than 100 manuscripts that were received in time were reviewed again for inclusion in both the bound and electronic volumes, the latter allowing us to include a few late submissions. The papers cover a spectrum of topics that represent a truly diverse nature of the field of materials science and engineering and related manufacturing processes. On behalf of the Organising Committee, we extend our warmest thanks and appreciation to the authors of the manuscripts, session chairs and sponsors for their interest, enthusiasm and support. Sincere thanks are also due to the technical editors, co-organisers and the members of the advisory committees, both local and international.

International Organisers

Prof. Debes Bhattacharyya
Centre for Advanced Composite Materials
Department of Mechanical Engineering
The University of Auckland
Auckland
New Zealand

Dr. Alan Kin Tak Lau
Centre of Excellence in Engineered Fibre Composites
Department of Mechanical Engineering
University of Southern Queensland
Toowoomba
Australia

Dr. Richard J.T. Lin
Centre for Advanced Composite Materials
Department of Mechanical Engineering
The University of Auckland
Auckland
New Zealand

Prof. Naresh Bhatnagar
Department of Mechanical Engineering
Indian Institute of Technology (IIT) Delhi
Hauz Khas, New Delhi 110 016
India

Prof. Tirumalai. S. Srivatsan
Division of Materials Science and Engineering
Department of Mechanical Engineering
The University of Akron
Akron, Ohio 44325-3903
USA

Organising Committee

Member	Affiliation	Country
Prof. Debes Bhattacharyya (Chair)	**University of Auckland**	**New Zealand**
Prof. Tirumalai S. Srivatsan	**University of Akron**	**USA**
Prof. Naresh Bhatnaghar	**Indian Institute of Technology, IIT (Delhi)**	**India**
Dr. Alan Kin-tak Lau	**Uni. of Southern Queensland**	**Australia**
Dr. Richard J.T. Lin (Secretary)	**University of Auckland**	**New Zealand**
Prof. Stoyko Fakirov	**University of Auckland**	**New Zealand**
Assoc. Prof. Simon Bickerton	**University of Auckland**	**New Zealand**
Assoc. Prof. Allan Easteal	**University of Auckland**	**New Zealand**
Dr. Sourish Banerjee	**University of South Queensland**	**Australia**
Dr. Mark Battley	**University of Auckland**	**New Zealand**
Dr. Raj Das	**University of Auckland**	**New Zealand**
Dr. Yu Dong	**University of Auckland**	**New Zealand**
Dr. Miro Duhovic	**IVW, University of Kaiserslautern**	**Germany**
Dr. Krishnan Jayaraman	**University of Auckland**	**New Zealand**
Dr. Jim Lee	**University of Auckland**	**New Zealand**
Dr. Dongyan Liu	**University of Auckland**	**New Zealand**
Dr. Xiaowen Yuan	**University of Auckland**	**New Zealand**
Dr. Sanjeev Rao	**University of Auckland**	**New Zealand**
Dr. Anjaneya Prasad Penneru	**University of Auckland**	**New Zealand**
Ms. Syamali Bhattacharyya	**Uniservices Ltd**	**New Zealand**
Ms. Sheeja Chidambaram	**University of Auckland**	**New Zealand**

International Advisory Committee

Member	Affiliation	Country
Prof. Suresh G Advani	**University of Delaware**	**USA**
Prof. Mathias Brieu	**Ecole centrale, Lille**	**France**
Prof. Klaus Friedrich	**Institut fuer Verbundwerkstoffe GmbH**	**Germany**
Prof. Anup Ghosh	**Indian Institute of Technology (IIT Delhi)**	**India**
Prof. Patricia Krawzak	**Ecole de Mine, Douai**	**France**
Prof. Anil Netravali	**Cornell University**	**USA**
Prof. Y.K.D.V.Prasad	**University of Queensland**	**Australia**
Dr. Dinesh Agarwal	**Pennsylvania State University**	**USA**
Dr. Manoj Gupta	**National University of Singapore**	**Singapore**
Dr. Satish Kailas	**Indian Institute of Science**	**India**
Dr. K.U. Kainer	**GKSS Research Center**	**Germany**
Dr. Kamal Kar	**Indian Institute of Technology (IIT Kanpur)**	**India**
Dr. Masaaki Nakai	**Tohoku University**	**Japan**
Dr. Mitsuo Niimoni	**Tohoku University**	**Japan**
Dr. John Yong Ming Shyan	**SIMTech**	**Singapore**
Dr. Raghavan Srinivasan	**Wright State University**	**USA**
Dr. S.K. Thakur	**Delphi Automotive Systems**	**Singapore**
Prof. Jens Schuster	**University of Applied Sciences Kaiserslautern**	**Germany**
Dr. Sébastien Comas-Cardona	**Ecole des Mines de Douai**	**France**

Local Advisory Committee

Member	Affiliation
Prof. John Chen	**University of Auckland**
Prof. Roy Crawford	**University of Waikato**
Prof. George Ferguson	**University of Auckland**
Prof. Wei Gao	**University of Auckland**
Dr. Mark Jones	**University of Auckland**
Dr. Michelle Dickinson	**University of Auckland**
Dr. Alan Fernyhough	**Scion**
Dr. Zhan Chen	**Auckland University of Technology**
Prof. Deliang Zhang	**University of Waikato**
Dr. Kim Pickering	**University of Waikato**
Dr. Mark P Staiger	**University of Canterbury**

Technical Editors

Member	Affiliation
Peter Lescher	**University of Auckland**
Ryan McCardle	**University of Auckland**
Peng Shaun Tan	**University of Auckland**

Plenary and Keynote Speakers

Member	Affiliation	Country
Prof. Roy Crawford	**University of Waikato**	**New Zealand**
Prof. Klaus Friedrich	**Institut fuer Verbundwerkstoffe GmbH**	**Germany**
Dr. Andrew Beehag	**CRC for Advanced Composite Structures**	**Australia**
Prof. Naresh Bhatnagar	**Indian Institute of Technology (IIT Delhi)**	**India**
Prof. Anil K Bhowmick	**Indian Institute of Technology (IIT Patna)**	**India**
Prof. Christoph Binetruy	**Ecole des Mines de Douai**	**France**
Prof. Ralph Cooney	**University of Auckland**	**New Zealand**
Prof. Alan Crosky	**University of New South Wales**	**Australia**
Prof. Pascal Hubert	**McGill University**	**Canada**
Prof. Eugene Joseph	**Virginia Tech**	**USA**
Prof. Karl U. Kainer	**GKSS Research Center**	**Germany**
Prof. Byung Sun Kim	**Korea Institute of Materials Science**	**Republic of Korea**
Prof. Alan Kin-Tak Lau	**University of Southern Queensland**	**Australia**
Prof. Woo Il Lee	**Seoul National University**	**Republic of Korea**
Prof. Peter Mitschang	**Institut für Verbundwerkstoffe GmbH**	**Germany**
Prof. Mitsuo Niinomi	**Tohoku University**	**Japan**
Prof. Robert Shanks	**RMIT University**	**Australia**
Prof. Tirumalai Srivatsan	**The University of Akron**	**USA**
Prof. Manfred Stamm	**Leibniz Institute of Polymer Research**	**Germany**
Prof. Norbert Stribeck	**University of Hamburg**	**Germany**
Prof. Ramesh Talreja	**Texas A&M University**	**USA**
Prof. Vikram Yadama	**Washington State University**	**USA**

Contents

Relating Performance and Structure of Advanced Nanocomposites by New Methods in Time-resolved X-Ray Scattering

Norbert Stribeck
Ahmad Zeinolebadi
Morteza Ganjaee-Sari
Institute of Technical and Macromolecular Chemistry,
University of Hamburg, Hamburg, Germany

Abstract

Extruded nanocomposites based on polyolefins are prepared in a joint European research project. They are monitored during mechanical fatigue tests by 2D X-ray scattering. Mechanical performance and structure parameters are determined. The structure evolution during the test is demonstrated in movies. The evaluation is based on newly developed automated data evaluation methods that are presented. The methods are adapted both to the study of thermoplastic materials that fail at rather low strains, and to the voluminous data series that are generated at modern synchrotron radiation sources. In wide-angle X-ray scattering the fiber patterns are automatically mapped into reciprocal space for a quantitative evaluation by peak integration in reciprocal space. In small-angle X-ray scattering pattern series are transformed to physical space, where distinct peaks show up that permit to monitor even small changes of nanostructure parameters by adapted methods. If cylindrical samples with a structure gradient are studied, a very fast tomographic method is presented that reconstructs the scattering patterns emanating from small volume elements along the fiber diameter. These patterns can be fed into the above mentioned automated wide- or small-angle algorithms for quantitative analysis.

Introduction

Technical progress in X-ray scattering

Intense, reliable X-ray sources and fast detectors are presently becoming generally available. At DESY in Hamburg, the PETRA III storage ring provides one of the most brilliant X-ray sources worldwide. At the PETRA III facility less than a second will be sufficient to expose a low-noise two-dimensional (2D) scattering pattern of polymer materials. Moreover, in detector development a similar break-through has been achieved [1, 2].

It may be objected that for a long time low-noise scattering curves can be recorded with repeat frequencies of several Hertz. Nevertheless, the value of those older data is limited. Either the material is exhibiting isotropic scattering – in this case a comprehensive analysis requires assumptions on the structure (e.g. the assumption of an ideal lamellar stack), or the material is anisotropic. In this case a single measured curve does not describe the complete scattering pattern, or the 2D pattern of the past is noisy. Applying the new technology it will become possible to exhaust the information content of X-ray scattering while monitoring the structure in *oriented* polymer materials in space and real time. A sweep of a polymer fiber by a microbeam will be possible in 30 s. Thus, spatial resolution and time resolution may be combined to study the response of different annular zones in a polymer fiber to, e.g. mechanical or thermal load.

Adapted data evaluation for materials with fiber symmetry

Parts with fiber symmetry – like fibers, rods or tubes – are not only of practical interest. Moreover, they appear particularly suited for investigation by means of scattering methods, because the recorded information is complete. As the part is rotated about its axis, the 2D scattering pattern does not change. Thus, there is no need to take patterns at different rotation angles, as it would be necessary for materials with less symmetry.

It is not sufficient to simply engage the novel instrument – the anticipated data must be adequately evaluated in due time, as well. In this respect two big problems arise. On the one hand, the data flood is increasing to such an extent that automated evaluation methods must be developed. On the other hand, the data structure has changed, in principal. Instead of scattering curves scattering images must be evaluated. The goal can be achieved by combining digital image processing and scattering theory [3]. In this paper several methods are presented that have recently been developed by us in order to quantitatively evaluate extensive sets of 2D scattering patterns from polymer materials with fiber symmetry.

Monitoring the WAXD of fibers under load

Motivation and method design

In wide-angle X-ray diffraction (WAXD) experiments the patterns must be mapped into reciprocal space before they can be analyzed quantitatively. For this purpose interactive computer programs [4, 5] are utilized that rest upon unnecessary [6] approximations. Such a design is no disadvantage in crystallography, because sophisticated interactive refinement methods are required anyway for the exact determination of crystal structure parameters in manageable series. In contrast, in materials science time-resolved experiments are frequent, and voluminous series of diffraction patterns must be processed. The materials scientist can tolerate minor inaccuracy of the mapping, if the experiment shall monitor the variation of peak intensity or shape. Because the fiber tilt may change during the experiment, the algorithm must be able to track and to compensate such variation. By revisiting the theoretical treatment of the fiber mapping it has been demonstrated [6]

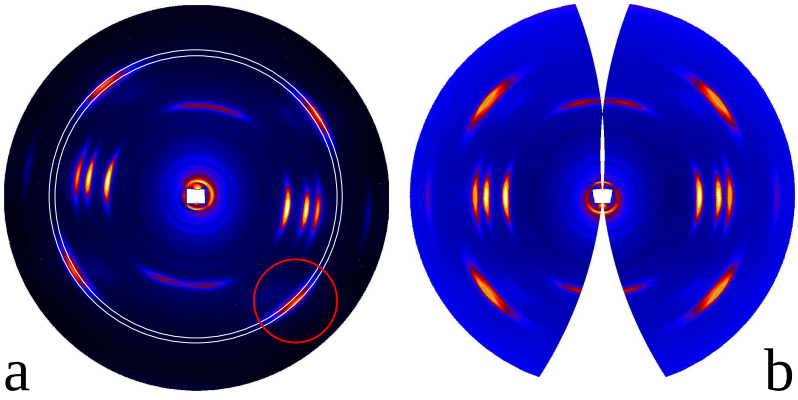

Figure 1: (a) Interactive mode of wf_premap: Draw the reflection circle through the centers of the reflection spots of an internal standard reflection (here: polypropylene (131) reflection), and widen the circle into a belt that contains the maxima of the reflection spots. Finally input 4 circles (one indicated). (b) The procedure `wf_map` has mapped the fiber diffraction pattern into reciprocal space

that there is no principal reason to refine an approximate center of the fiber pattern iteratively. Moreover, instead of an approximation [7, 8] of the tilt angle β of the fiber an exact equation [6] can be employed. In the methodical paper [9] an algorithm is presented by which the mapping can be performed automatically. Its design rests on the application of the mentioned findings. Intricate parametrization is simplified, and slow trigonometric functions are avoided to a large extent. If inaccuracies of 2 pixels can be tolerated, a pattern is automatically mapped into reciprocal space in real time.

For each series of diffraction patterns from a time-resolved experiment, some geometrical parameters must once be determined interactively. Our procedure `wf_premap` assumes that the studied material exhibits a sharp reflection that is located neither on the equator nor on the meridian. In the example we investigate polypropylene and select the (131) reflection as the internal standard. With the crystallographic c-axis parallel to the meridian, the reflection is characterized by the parameters [10] $d_{hk\ell} = d_{131} = 0.406\,\mathrm{nm}$ and by $c/\ell = 0.6504\,\mathrm{nm}$ that defines the position of the reflection ring on the Polanyi sphere [6, 11, 12]. The wavelength of X-radiation (here: $\lambda = 0.15\,\mathrm{nm}$) must be known, too. Now the first pre-mapping run of the series is started by

```
wave>ab = wf_premap(ss,a,0.15,0.406,0.6504)
```

The procedure requires a diffraction pattern as input (`a`). It generates output both in a “save-set” (`ss`), and in a background-corrected diffraction pattern (`ab`). When started for the first time, the procedure enters interactive mode and the user is presented the pattern as shown in Fig. 1a. The result of the mapping is shown in Fig. 1b.

Application

In an application, uniaxially oriented polypropylene (PP) is molten and crystallized isothermally from the oriented, quiescent melt. The results [13] show that nucleation and growth of differently oriented sets of crystallites (c-set and a^*-set) are decoupled. After shallow quench crystallization is preceded by (spinodal) decomposition. Peak integrals ($\rightarrow$crystallinity) and minimum crystallite

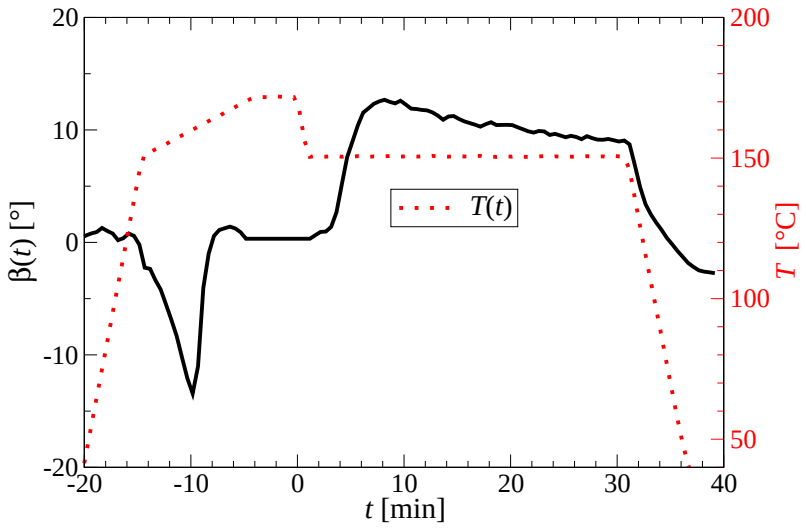

Figure 2: Tilt-angle tracking curve $\beta\,(t,T)$ from the automatic fiber-mapping procedure in an experiment in which β is changing considerably

size are tracked. In the commercial starting material a^*-set crystallites melt at 158°C. The *c*-set melts at 170°C furnace temperature. After recrystallization both sets melt at 170°C. Isothermal crystallization is divided in two distinct phases. During nucleation the crystallinity stays low. The second phase is dominated by crystallinity growth. At 150°C the *c*-set is seeded first. At 145°C and 140°C a^*-oriented crystallites are the first. The first-seeded set starts to grow first, as well. *c*-set crystallinity is always growing faster than a^*-set crystallinity. The evolution of the corresponding SAXS [14] cross-diagram in the growth phase can both be explained by lamellae growing at right angles, and by block merging.

Figure 2 shows $\beta\,(t,T)$ of one of the experiments. The tracking curve appears smooth and demonstrates the reliability of the tilt-angle determination. Tilt-angle variation is an issue, because the oriented PP film is heated until it becomes a viscous melt. Consequently, the sample shrinks and bends in the synchrotron X-ray beam.

After the mapping the intensity distribution is known almost everywhere in reciprocal space except for a wedge region near the meridian (cf. Fig. 1b). Thus, reflection intensities can readily be integrated in reciprocal space, where the relation between scattering and structure is clear from scattering theory [3, 13]. Based on these integrals structural parameters can be computed that are well-founded from theory [13].

Figure 3 shows the evolution of weight crystallinities of the two sets of crystallites at 3 different crystallization temperatures. Latency periods between the quench and the start of the crystallization, as well as crystallization velocities of the two kind of crystallites can be extracted from these data. Finally, conclusions concerning the crystallization mechanisms can be drawn ([13]).

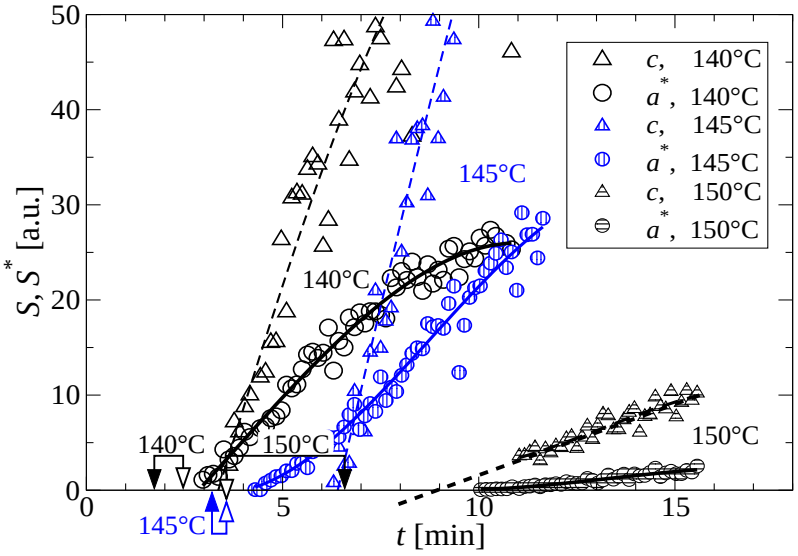

Figure 3: Evolution of relative weight crystallinities S, and S^* of c-oriented crystallites (dashed regression lines) and a^*-oriented crystals (solid regression lines), resp. during isothermal, oriented crystallization of hard-elastic PP from a quiescent melt as a function of crystallization temperature. Double-head arrows pointing at the t-axis indicate the first sighting of the a^*-set (full arrow head), and of the c-set (open arrow head), respectively

X-Ray scattering fiber tomography

Motivation

The structure inside a polymer part is not necessarily homogeneous. With fibers, extrudates, and latex particles [15] frequently a core-shell structure is reported. Moreover, engineers deliberately generate structure gradients in polymer parts for special functionality [16, 17]. If such a part is irradiated by an X-ray beam, the recorded pattern is an integral superposition of all the SAXS patterns emerging from the sequence of volume elements (voxels) along the beam path. From the mathematical point of view such a superposition is a projection which is of inferior value for the study of graded materials.

A first step towards a study of structure gradients has been the development of the X-ray microbeam technique [18–20]. Here only the diameter of the beam is limiting the lateral spatial resolution. Nevertheless, the longitudinal spatial resolution is simply the thickness of the sample. Microbeam scanning experiments in particular of fibers have been performed for many years and the raw data have been discussed, although the corresponding shortcoming has been known [21]. The solution of the problem is tomographic reconstruction. Problems arise from the fact that scattering patterns are multidimensional data but not simply a number (like the absorption in classical tomography). Thus, approximate tomographic reconstruction of scattering data with a manageable amount of artifacts is difficult. An exception is the case of part with uniaxial symmetry. In this case a reconstruction of the scattering patterns is possible that would have emerged from individual voxels in a plane perpendicular to the “fiber” axis [22]. Nevertheless, this method is only of academic value. The exposure time for the recording of scattering data of one cross-section of the

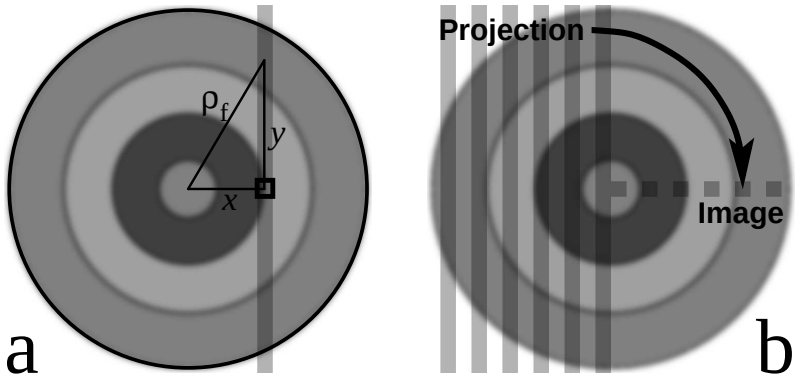

Figure 4: (a) Fiber cross-section irradiated by an X-ray beam at an offset x from its center. The structure $\rho\left(\rho_f\right)$ shows fiber symmetry. From all structures along the beam path a superposition is probed. y is the variable of the integration. (b) One-dimensional tomographic reconstruction turns the measured series of *projected* scattering patterns into the *image* patterns from voxels (quadratic boxes) on the fiber radius

part is in the order of days [22].

Introduction of the method

A more practical tomographic method can be applied, if the part to be studied both exhibits macroscopic fiber symmetry, and the structure only varies as a function of the distance from its central axis. By means of this method fibers, pipes, and extruded strands can be investigated. Thus, we call it "X-ray scattering fiber computer tomography" (XSF-CT). A complete set of projected scattering patterns is collected in a single microbeam scan across the fiber, because the set of projections does not change as the sample is rotated about its axis. Such an experiment is completed in about 30 min. Moreover, compared to the general tomography the mathematics of image reconstruction is simplified. A set of 40 measured scattering patterns is reconstructed in typically less than 10 min.

In a general tomographic X-ray experiment [23], a voluminous sample is scanned by a thin X-ray beam. As a function both of the position x of the scanning beam on the sample, and of the sample rotation angle ϕ, projections (notation: $\{\,\}$) of the absorption $\{A\}(x,\phi)$ or even of complete scattering patterns $\{I\}(\mathbf{s},x,\phi)$ are measured, in order to analyze the structure variation in the plane of the sample that is scanned by the X-ray beam [22, 24, 25]. Here $\mathbf{s}$ is the scattering vector with $|\mathbf{s}| = s = (2/\lambda)\sin\theta$, the X-ray wavelength λ and the scattering angle 2θ. In the examples mentioned, a tomographic image reconstruction [23, 26, 27] returns either the spatial variation of the X-ray absorption in the plane, or of the scattering emanating from the resolved voxels in the plane. The smearing caused from projection is eliminated by application of the Fourier transform theory, and a clear image of the inner structure is obtained.

The fundamental geometry is sketched in Fig. 4a. The information in the measured signal $\{A\}(x)$ or $\{I\}(\mathbf{s},x)$, respectively, does not represent the sought information $A(x)$ or $I(\mathbf{s},x)$ originating from the small square (voxel) around the position x. Instead, to a first approximation it is represented by the projection integral

$$\{I\}(\mathbf{s},x) \quad = \quad 2\int_x^\infty I\left(\mathbf{s},\sqrt{x^2+y^2}\right)dy \tag{1}$$

$$= \quad 2\int_x^\infty \frac{I(\mathbf{s},\rho_f)\,\rho_f\,d\rho_f}{\sqrt{\rho_f^2-x^2}}. \tag{2}$$

Eq. (1) is the definition of the Abel transform [27]. In X-ray scattering Eq. (1) is established textbook knowledge [3, 28–33]. There it describes the slit smearing. Even the inverse Abel [34] transform

$$I(\mathbf{s},x) \quad = \quad -\frac{1}{\pi}\int_0^\infty \frac{d\{I\}(\mathbf{s},\rho_f)}{d\rho_f}\frac{dy}{\rho_f} \tag{3}$$

$$= \quad -\frac{1}{\pi}\int_x^\infty \frac{d\{I\}(\mathbf{s},\rho_f)}{d\rho_f}\frac{d\rho_f}{\sqrt{\rho_f^2-x^2}}, \tag{4}$$

is in scattering textbooks since Guinier [35] and DuMond [36]. Similar to the filtered backprojection algorithm of the general tomography, low-noise reconstruction algorithms [37–39] for the tomography of materials with cylindrical symmetry are readily available from the field of "one-dimensional tomography". The principle of one-dimensional tomographic reconstruction is sketched in Fig. 4b. Here we implicitly assume that the scattering from every irradiated voxel in the fiber shows fiber symmetry itself (local fiber symmetry). Otherwise characteristic reconstruction aberrations are expected [22, 40]. Deviations from local fiber symmetry cause restricted or shifted visibility of scattering features along the fiber radius. These aberrations are detected in the reconstructed image and result in additional information on the structure inside the fiber [40].

Application

In a feasibility study [40] precursors of polymer microfibrillar-reinforced composites (MFC) containing poly(ether)-*block*-amide (PEBA) and poly(ethylene terephthalate) (PET) with varying cold-draw ratio are studied. The results from a direct analysis of the smeared measured patterns are compared to results obtained after tomographic reconstruction.

Data are presented from a cold-drawn (draw ratio $\lambda_d \approx 3$) co-extrudate of 70 wt.-% PEBA and 30 wt.-% PET (abbreviated: MFC73). In the scanning-microbeam experiment the strand shows an isotropic long period and an equatorial streak at almost every beam position (Fig. 5, left column). Only the tomographically reconstructed patterns (right column) exhibit that the long-period ring-reflection is not present in the core of the fiber. As the feature becomes visible, it first shows up at the equator. With increasing distance from the fiber axis, reflection arcs are growing towards the meridian. Above $\rho_f = 300\,\mu$m the arcs join into a closed circle. Because such behavior has been observed with neat PEBA as well, this orientation phenomenon is not indicating some interaction between the PEBA and the PET microfibrils. The reconstructed central voxel ($\rho_f = 0$) is dominated by one of the reconstruction aberration effects (from voxels with tangential grain) [40]. Examination of the equatorial streak exhibits only in the reconstruction that it grows broader towards the center of the fiber. The streak is allocated to needle-shaped domains, and is only observed with strands from co-extruded blends. If these needles are thin PET microfibrils, the tomography shows that in the center of the fiber these microfibrils are shorter than in an intermediate region. The structure gradient in the outer region of the strand is discussed in the original paper [40].

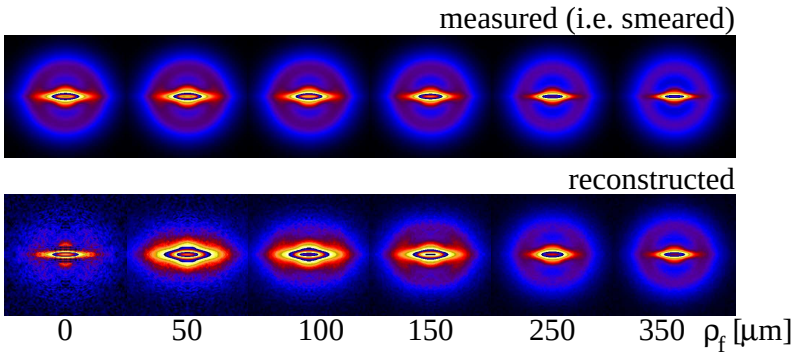

Figure 5: Cold-drawn ($\lambda_d \approx 3$) MFC73 in a scanning microbeam experiment. Measured scattering intensity $\{I\}\left(s_{12}, s_3, \rho_f\right)$ (top row) and reconstructed scattering $I\left(s_{12}, s_3, \rho_f\right)$ (bottom row) for short distances ρ_f from the fiber axis. The patterns display the range $-0.1\,\mathrm{n}m^{-1} \leq s_{12}, s_3 \leq 0.1\,\mathrm{n}m^{-1}$ in uniform logarithmic scale ($s = (2/\lambda)\sin\theta$)

SAXS monitoring of mechanical tests

Motivation and method development

Advanced polymer materials are urgently sought after e.g. in automotive industry in order to accomplish the goals of climate protection by reduction of weight. Such newly engineered materials have to prove their serviceability in mechanical tests. Classical tensile tests are performed to determine the modulus and ultimate properties. Load cycling experiments are carried out to determine the fatigue behavior. In order to reveal the mechanisms of, e.g., failure or fatigue, it is desirable to monitor mechanical tests by SAXS. In this way the response of the nanostructure to mechanical load is revealed.

Results

In a feasibility study [41] slow continuous mechanical tests of oriented PP are monitored by SAXS and quantitatively evaluated. A continuous-strain test exhibits fracture and release of weak lamellae (2 - 10% strain). Beyond that conversion of lamellae into needles is observed. As all layers are consumed, the material breaks. Fatigue is studied in a load-reversal experiment (between 10% and 35% strain, Fig. 6). In each cycle crystallization, layer break, and relaxation melting are observed. Figure 7 presents the result. The top chart shows the macroscopical strain, $\varepsilon(t)$, imposed to the material and measured at the point of X-ray irradiation. The four load-reversal cycles are easily identified. The chart in the middle reports the extracted nanostructure parameters, $L(t)$, $e_{cac}(t)$, and $S(t)$. The bottom diagram presents the macroscopic resistance, $\sigma(t)$, which the material is opposing to strain. The figure shows that crystallization, rupture of lamellae and melting of fragments are continuously reshaping the domains of the PP material in the cycles of the fatigue test. The long-period cycle exhibits a phase shift with respect to the imposed strain cycling. Moreover, there is an indication of amplitude attenuation. Fatigue is demonstrated in the curve $\sigma(t)$ by decreasing stress peaks. An in-depth discussion of the zones indicated in Fig. 7 is in the original paper [41]. In particular, the combination of SAXS and fatigue test shows the transition from stress-induced crystallization to crystallite rupture $\sigma(t) \approx 20$ MPa.

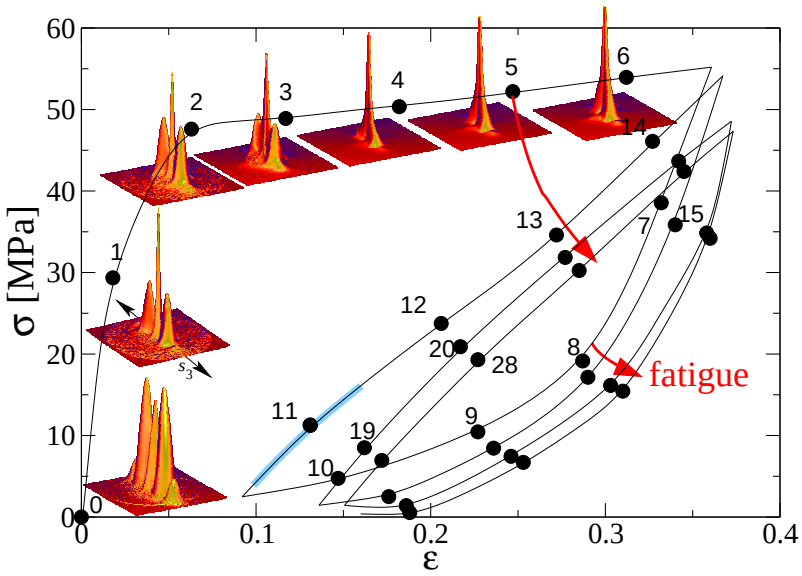

Figure 6: Oriented PP. Load cycling monitored by SAXS. Circular dots show where SAXS patterns have been recorded. Numerical labels indicate their sequence. The drawing direction with respect to the patterns, s_3, is indicated by a double-head arrow

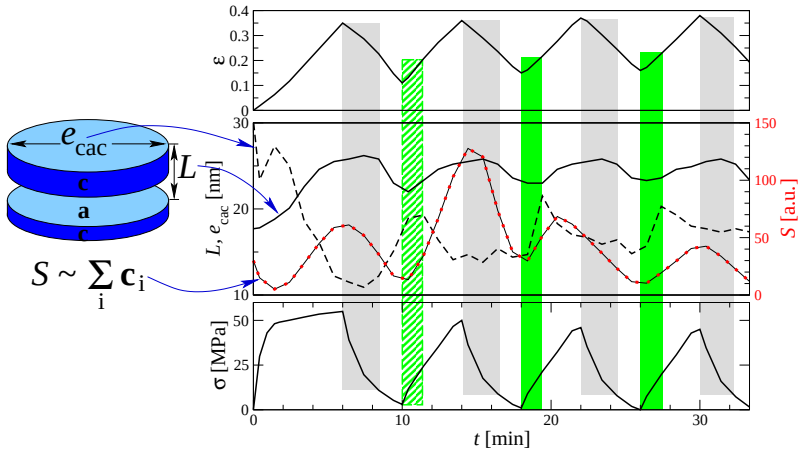

Figure 7: Dynamic load-reversal mechanical test of hard-elastic PP film. As a function of the elapsed time t the macroscopic parameters strain, ε (top graph), and tensile stress, σ (bottom graph) are displayed together with topological nanostructure parameters (middle). In the middle diagram the solid line shows the long period, L. The broken line displays the lateral extension, e_{cac}, of a sandwich made from two crystalline lamellae. The line with circular dots exhibits the variation of the strength, S, of the CDF. Vertical bars indicate zones of strain-induced crystallization (dark) and relaxation-induced melting (light), respectively

Conclusions

Considering the present instrumental development at synchrotron radiation facilities the development of advanced data evaluation methods appears to be both promising and necessary in order to master the future data flood. The 3 presented methods demonstrate the potential of such work. In order to discharge the user, a part of the data evaluation may be carried out at the synchrotron facility. Such added service would require not only computing power, but also additional manpower. In addition to the beamline scientist an evaluation specialist would become necessary. It would be his job to detect if raw data must be smoothed. He would have to eliminate the machine background, would generate detector masks, would center and align each scattering pattern and would fill blind areas from consideration of symmetry. As an added service, the community of the evaluation specialists could select some standard experiments for which complete user-friendly programming environments could be built. Nevertheless, for the predominant fraction of individually designed setups it will remain necessary for the polymer scientist himself to familiarize with adapted programming techniques. This will be of particular importance, if methods shall be developed that grow with the growth of instrumental capacity. Ultimately, it is expected that an increase of the quality of results returned from scattering experiments will closely be correlated to the manpower dedicated to the programming of data evaluation modules.

Acknowledgements. The authors thank the Hamburg Synchrotron Radiation Laboratory (HASYLAB) for beam time granted in the frame of project II-20080015. Development of the reported methods has been supported by the 7th framework program of the European Union (Project NANOTOUGH FP7-NMP-2007-LARGE-2.1.1).

References

[1] Broennimann C., Eikenberry E.F., Henrich B., Horrisberger R., Hülsen G., Pohl E., Schmitt B., Schulze-Briese C., Suzuki M., Tomizaki T., Toyokawa A., Wagner A.: The pilatus 1m detector. J. Synchrotron Rad., **13**, 120–130 (2006).

[2] Hülsen-Bollier G.: The PILATUS 1M Detector. A Novel Large Area Pixel Detector. Ph.D. thesis, Dept. Physics, University of Erlangen-Nürnberg, Germany (2005).

[3] Stribeck N.: X-Ray Scattering of Soft Matter. Springer, Heidelberg, New York (2007).

[4] Rajkumar G., AL-Khayat H., Eakins F., He A., Knupp C., Squire J.: Fibrefix - a new integrated ccp13 software package. Fibre Diffraction Rev., **13**, 11–18 (2005).

[5] Bian W., Wang H., McCullough I., Stubbs G.: Wcen: a computer program for initial processing of fiber diffraction patterns. J. Appl. Cryst., **39**, 752–756 (2006).

[6] Stribeck N.: On the determination of fiber tilt angles in fiber diffraction. Acta Cryst., **A65**, 46–47 (2009).

[7] Franklin R.E., Gosling R.G.: The structure of sodium thymonucleate fibres. ii. cylindrically symmmetrical patterson function. Acta Cryst., **6**, 678–685 (1953).

[8] Fraser R.D., Macrae T.P., Miller A., Rowlands R.J.: Digital processing of fibre diffraction patterns. J. Appl. Cryst., **9**, 81–94 (1976).

[9] Stribeck N., Nöchel U.: Direct mapping of fiber diffraction patterns into reciprocal space. J. Appl. Cryst., **42**, 295–301 (2009).

[10] Mencik Z.: Crystal structure of isotactic polypropylene. J. Macromol. Sci. Phys., **B6**, 101–115 (1972).

[11] Polanyi M.: Das röntgen-faserdiagramm i. (the x-ray fiber-diagram i.). Z. Phys., **7**, 149–180 (1921).

[12] Polanyi M., Weissenberg K.: Das röntgen-faserdiagramm ii. (the x-ray fiber-diagram ii.). Z. Physik, **9**, 123–130 (1923).

[13] Stribeck N., Nöchel U., Funari S.S.: Melting and crystallization of differently oriented sets of crystallites in hard-elastic polypropylene. Macromolecules, **42**, 2093–2101 (2009).

[14] Stribeck N., Nöchel U., Almendárez Camarillo A., Roth S.V., Dommach M., Bösecke P.: Saxs study of oriented crystallization of polypropylene from a quiescent melt. Macromolecules, **40**, 4535–4545 (2007).

[15] Dingenouts N., Bolze J., Potschke D., Ballauff M.: Analysis of polymer latexes by small-angle x-ray scattering. Adv. Polym. Sci., **144**, Epoxide Resins, Polyampholytes), 1–Epoxide Resins, Polyampholytes),47 (1999).

[16] Kieback B., Neubrand A., Riedel H.: Processing techniques for functionally graded materials. Mater. sci. eng. A Struct. mater. prop. microstruct. proces., **362**, 81–106 (2003).

[17] Pompe W., Worch H., Epple M., Friess W., Gelinsky M., Greil P., Hempel U., Scharnweber D., Schulte K.: Functionally graded materials for biomedical applications. Mater. sci. eng. A Struct. mater. prop. microstruct. proces., **362**, 40–60 (2003).

[18] Riekel C., Engström P.: Diffraction and diffuse scattering from materials with microfocussed x-rays. Nuclear Instr. Meth. Phys. Res., **B97**, 224–230 (1995).

[19] Waigh T.A., Donald A.M., Heidelbach F., Riekel C., Gidley M.J.: Analysis of the native structure of starch granules with small angle x-ray microfocus scattering. Biopolymers, **49**, 91–105 (1999).

[20] Kolb R., Wutz C., Stribeck N., v. Krosigk G., Riekel C.: Investigation of secondary crystallization of polymers by means of microbeam x-ray scattering. Polymer, **42**, 5257–5266 (2001).

[21] Paris O., Li C., Siegel S., Weseloh G., Emmerling F., Riesemeier H., Erko A., Fratzl P.: A new experimental station for simultaneous x-ray microbeam scanning for small- and wide-angle scattering and fluorescence at bessy ii. J. Appl. Cryst., **40**, s466–s470 (2007).

[22] Stribeck N., Almendarez Camarillo A., Nöchel U., Schroer C., Kuhlmann M., Roth S.V., Gehrke R., Bayer R.K.: Volume-resolved nanostructure survey of a polymer part by means of saxs microtomography. Macromol. Chem. Phys., **207**, 1239–1249 (2006).

[23] Bonse U., Busch F.: X-ray computed microtomography (μct) using synchrotron radiation. Prog. Biophys. Molec. Biol., **65**, 133–169 (1996).

[24] Schroer C.G., Kuhlmann M., Roth S.V., Gehrke R., Stribeck N., Almendarez Camarillo A., Lengeler B.: Mapping the local nanostructure inside a specimen by tomographic small-angle x-ray scattering. Appl. Phys. Lett., **88**, 164102 (2006).

[25] Schroer C.G., Kuhlmann M., Günzler T.F., Benner B., Kurapova O., Patommel J., Lengeler B., Roth S.V., Gehrke R., Snigirev A., Snigireva I., Stribeck N., Almendárez Camarillo A., Beckmann F.: Full-field and scanning microtomography based on parabolic refractive x-ray lenses. Proc. SPIE, **6318**, 6318H (2006).

[26] Kak A.C., Slaney M.: Principles of Computerized Tomographic Imaging. IEEE Press, New York (1999).

[27] Bracewell R.: The Fourier Transform and Its Applications. Mc Graw-Hill, New York, 3rd edn. (1999).

[28] Guinier A., Fournet G.: Small-Angle Scattering of X-Rays. Chapman and Hall, London (1955).

[29] Hosemann R., Bagchi S.N.: Direct Analysis of Diffraction by Matter. North-Holland, Amsterdam (1962).

[30] Alexander L.E.: X-Ray Diffraction Methods in Polymer Science. Wiley, New York (1979).

[31] Glatter O., Kratky O. (eds.): Small Angle X-ray Scattering. Academic Press, London (1982).

[32] Feigin L.A., Svergun D.I.: Structure Analysis by Small-Angle X-Ray and Neutron Scattering. Plenum Press, New York (1987).

[33] Baltá Calleja F.J., Vonk C.G.: X-Ray Scattering of Synthetic Polymers. Elsevier, Amsterdam (1989).

[34] Abel N.H.: Auflösung einer mechanischen aufgabe. J. Reine Angew. Math., **1**, 153–157 (1826).

[35] Guinier A., Fournet G.: Correction of measurments of low-angle x-ray scattering. Nature, **160**, 501 (1947).

[36] DuMond J.W.M.: Method of correcting low angle x-ray diffraction curves for the study of small particle sizes. Phys. Rev., **72**, 83–84 (1947).

[37] Bitter I., Kaufman A.E., Sato M.: Penalized-distance volumetric skeleton algorithm. IEEE Trans. Visualization and Computer Graphics, **7**, 195–206 (2001).

[38] Dasch C.J.: One-dimensional tomography: a comparison of abel, onion-peeling, and filtered backprojection methods. Applied Optics,, **31**, 1146–1153 (1992).

[39] Dribinski V., Ossadtchi A., Mandelshtam V.A., Reisler H.: Reconstruction of abel-transformable images: The gaussian basis-set expansion abel transform method. Rev. Sci. Instr., **73**, 2634–2642 (2002).

[40] Stribeck N., Nöchel U., Fakirov S., Feldkamp J., Schroer C., Timmann A., Kuhlmann M.: Saxs-fiber computer-tomography. method enhancement and analysis of microfibrillar-reinforced composite precursors from pebax and pet. Macromolecules, **41**, 7637–7647 (2008).

[41] Stribeck N., Nöchel U., Funari S.S., Schubert T., Timmann A.: Nanostructure evolution in polypropylene during mechanical testing. Macromol. Chem. Phys., **209**, 1992–2002 (2008).